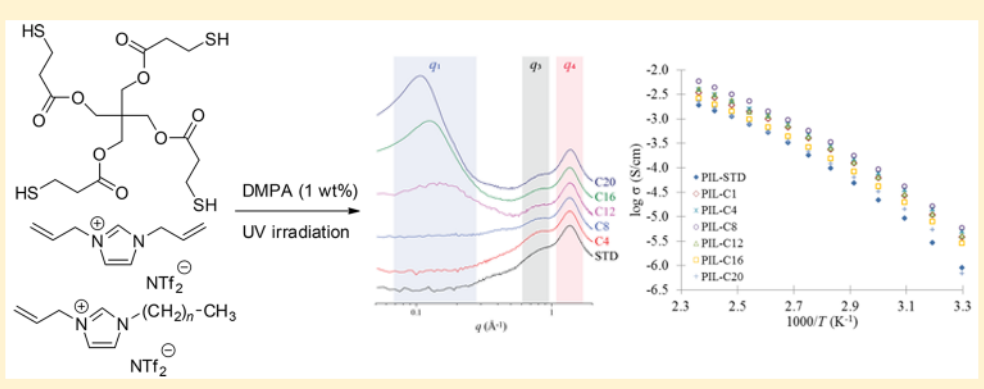


Thermomechanical and Conductive Properties of Thiol-Ene Poly(ionic liquid) Networks Containing Backbone and Pendant **Imidazolium Groups**

Abigail F. Bratton, Sung-Soo Kim, Soo Christopher J. Ellison, and Kevin M. Miller

Supporting Information



ABSTRACT: A series of covalently cross-linked poly(ionic liquid) networks were prepared using thiol-ene "click" photopolymerization. In these networks, imidazolium groups are placed in the backbone and pendant to the main chain, creating a "hybrid"-type network architecture. The pendant imidazolium groups were incorporated into the networks from monofunctional "ene" monomers that contained either a terminal alkyl group at the imidazolium N-3 position of variable length (R = C1, C4, C8, C12, C16, or C20) or a variable alkyl tether spacer (n = 6 or 10) between the newly formed sulfide and the imidazolium ring. Thermal characterization of these networks indicated a general decrease in $T_{\rm g}$ as the length of the terminal alkyl chain length increased from C1 to C8, followed by an abrupt increase in Tg up to C20 due to increased van der Waals interactions between longer chains. X-ray scattering data confirmed the presence of chain-extended crystallites within the network cavities for the C16 and C20 systems, leading to the observed increase in $T_{\rm g}$ and the appearance of a melting transition for both systems. Ionic conductivities of the PIL networks were determined from dielectric relaxation spectroscopy (10⁻⁶ to 10^{-7} S/cm at 30 °C, 30% RH), and a direct correlation with polymer T_g was found.

INTRODUCTION

Poly(ionic liquid)s (PILs) combine the best attributes of ionic liquids (high thermal and electrochemical stability, ion conducting properties, etc.) with those from various polymeric architectures (mechanical stability, processability, viscoelasticity, etc.).1-4 A broad range of thermal, mechanical, and electrochemical properties are afforded by the numerous cations (imidazolium, triazolium, phosphonium, ammonium, etc.), anions (halides, inorganics, perfluorinated sulfonamides, etc.), and polymer microstructures (homopolymers, random copolymers, block copolymers, branched structures, networks and gels) that are available. As a result, PILs have been utilized in a variety of applications, including gas separation technologies, 5-8 anion exchange membranes, 9,10 sensors and actuators, 11,12 batteries, 13-16 and supercapacitors. 17 Due to the continued expansion of synthetic possibilities and potential end-use applications, the need to understand the fundamental structure-property relationships that underlie PIL behavior is becoming increasingly critical to maximizing performance.

The majority of the imidzolium PIL literature has focused on placing the charged group pendant to the polymer backbone through the polymerization of vinyl-, (meth)acrylic-, or styrenyl-substituted ionic liquid monomers. Within this vast array of "pendant PILs," the general consensus is that incorporation of long, flexible side chains or tethers (alkyl or

Received: September 26, 2018 Revised: October 31, 2018 Accepted: November 2, 2018 Published: November 2, 2018

Department of Chemistry, Murray State University, 1201 Jesse D. Jones Hall, Murray, Kentucky 42071, United States

^{*}Department of Chemical Engineering and Materials Science, University of Minnesota, 421 Washington Avenue SE, Minneapolis, Minnesota 55455, United States

Korea Institute of Science and Technology, Institute of Advanced Composite Materials, 92 Chudong-ro, Bongdong-eup, 55324, Republic of Korea

ethyleneoxy) coupled with large, noncoordinating anions such as bis(trifluoromethylsulfonyl)imide [NTf2] provides the most promising overall ionic conductivities by diminishing $T_{\rm g}$ and ionic aggregation through structural relaxation. From a mechanistic perspective, recent atomistic molecular dynamic simulations by Ganesan et al. investigated three potential mechanisms for ion transport in the pendant PIL poly(1-butyl-3-vinylimidazolium) [PF6] and found that intramolecular ion hopping was predicted to occur greater than 97% of the time; however it remains to be seen if this is a general feature of all pendant PIL systems. Throughout all of these studies, it has become imperative that ionic conductivity and structural dynamics be decoupled in order to understand the complex relationships that exist between the polymer nanostructure and ion transport mechanisms.

Step-growth PIL architectures, where the charged group is placed directly into the backbone ("backbone PILs"), may provide an answer to reducing ionic aggregation since the charged groups can be anchored into the backbone in a precise fashion by controlling spacer lengths. Long and co-workers prepared segmented, imidazolium-containing block copolymers by first reacting dibromoalkanes with sodium imidazole, followed by coupling with a PTMO macromonomer.³⁵ Data acquired from differential scanning calorimetry (DSC) and multiangle X-ray scattering (MAXS) experiments indicated the presence of microphase separation. In another example, Gibson and co-workers discussed the thermal and conductive properties of a series of imidazolium-containing polyesters, prepared from imidazolium-containing diols and diacid chlorides.³⁶ The resulting PILs exhibited impressive conductivities of up to 10^{-5} S/cm at 25 °C. Backbone PIL segmented polyurethanes, prepared from imidazolium-containing diols, 37,38 and block copolymers of polycaprolactone and imidazolium-containing diols³⁹ have also been reported with conductivities on the order of 10⁻⁵ to 10⁻⁷ S/cm at 25 °C. Throughout these studies, a continuous effort has been made to carefully control the spacer distance between charged groups in an attempt to create a more continuous ionic matrix, the importance of which was recently explored by Segalman.⁴ In their work, an imidazolium-containing "backbone PIL" was found to exhibit a 10-fold increase in T_g -independent ionic conductivity when compared with a "pendant PIL" counterpart.40 The large enhancement in conductivity was attributed in part to a more uniform distribution of IL groups throughout the polymer (termed "percolated aggregates"), resulting in more efficient ion transport. This hypothesis was supported by wide-angle X-ray scattering (WAXS) data, which indicated longer-range anion-anion correlations in the "backbone PIL" as evidenced from a lowering of the anion-anion q value. The concept of percolated aggregates in backbone PILs has also been theorized as a result of several simulation studies. 41-43

Our contributions to the field of PILs have focused on covalently cross-linked, imidazolium-containing "backbone" PIL networks, prepared from step-growth polymerization strategies. Reports of PIL networks are rare due to the presumed restrictive nature that cross-linking has on ion mobility/transport and thus conductivity; however, the enhanced mechanical properties associated with network formation could be advantageous in a number of the aforementioned applications. Initial synthetic efforts utilized base-catalyzed Michael addition polymerization to generate covalently cross-linked, polyester PIL networks from imidazolium-containing acetoacetate monomers and diacrylates. 44,45

The highly cross-linked networks that stemmed from these studies exhibited a wide range of $T_{\rm g}$ values with high moduli (>4 MPa at 100 °C) and ionic conductivities (10^{-6} to 10^{-8} S/cm at 25 °C, 30% RH), which were comparable to or improvements over other, non-network, imidazolium-containing PILs. $^{3,36-39}$

More recently, we have employed thiol-ene "click" photochemistry as a more efficient and atom economical method for preparing covalently cross-linked PIL networks.⁴⁶ An initial set of PIL networks with variable cross-link density, prepared from 1,3-bisallylimidazolium [NTf2] and commercially available thiol cross-linkers, exhibited a wide range of thermal and mechanical properties with encouraging ionic conductivities (10^{-5} to 10^{-7} S/cm at 25 °C, 30% RH). In an effort to improve the ionic conductivity of these initial thiolene PIL networks, a series of materials are reported here where monofunctional, imidazolium-containing "ene" monomers were incorporated in order to reduce $T_{\rm g}$ and cross-link density while keeping the IL concentration relatively high. The overall thiol/ene functional group ratio was held stoichiometric across all polymerizations. The resulting materials were networks which contained both pendant and backbone imidazolium groups ("hybrid" PIL networks). Monofunctional "ene" monomers utilized in these networks contained either a terminal alkyl group on the imidazolium ring at N-3 of variable lengths (R = C1, C4, C8, C12, C16, or C20) or a variable alkyl tether spacer (n = 6 or 10) between the newly formed sulfide linkage and the imidazolium ring. Structure-activity relationships, as they relate to the thermal, mechanical, and conductive properties of the networks, are discussed below, and X-ray scattering data were also acquired to learn more about the unique nanostructure of these PILs.

EXPERIMENTAL SECTION

Materials. All chemicals were purchased from Sigma-Aldrich or Acros Organics and were used as received without further purification. Pentaerythritol tetrakis(3-mercaptopropionate) (PTMP, > 95%) was placed in a high vacuum oven (50 $^{\circ}$ C, < 0.01 mmHg) for 48 h prior to use. An ELGA Purelab Ultra filtration device produced ultrapure water having a resistivity of 18 MΩ·cm. The preparation of 1,3-bisallylimidazolium [NTf₂] has been previously described.⁴⁶

Monomer Characterization. ¹H and ¹³C NMR spectra were obtained on a JEOL-ECS 400 MHz spectrometer, and reported chemical shift values were referenced to residual solvent signals (DMSO-*d*₆: ¹H, 2.50 ppm; ¹³C, 39.52 ppm). Relevant NMR spectra are included in the Supporting Information (Figures S1–S7). Elemental analyses were completed on a PerkinElmer 2400 CHNS/O Series II Elemental Analyzer.

Preparation of 1-Allyl-3-alkylimidazolium bis-(trifluoromethylsulfonyl)imide [NTf₂] Monomers 1a-1f. The preparation of 1-allyl-3-methylimidazolium bis-(trifluoromethylsulfonyl)imide [NTf₂] 1a has been previously reported.⁴⁷ The remaining 1-allyl-3-alkylimidazolium bis-(trifluoromethylsulfonyl)imide [NTf₂] ionic liquid monomers 1b-1f were prepared following the general procedure described below, which is specific for 1-allyl-3-butylimidazolium [NTf₂] 1b. Detailed synthetic procedures for ionic liquid monomers 1c-1f, including complete characterization data, can be found in the Supporting Information.

N-Allylimidazole (5.00 g, 0.0462 mol) was dissolved in acetonitrile (70 mL) with magnetic stirring. 1-Bromobutane

(6.65 g, 0.486 mol) was added, and the resulting homogeneous solution was warmed to 60 °C and stirred overnight. The volatiles were then removed under reduced pressure to afford 1-allyl-3-butylimidazolium bromide as a light yellow oil (10.9 g, 96%). ¹H NMR (400 MHz, DMSO- d_6): δ 9.30 (1 H, s), 7.87 (1 H, s), 7.77 (1 H, s), 6.04 (1 H, m), 5.36 (2 H, m), 4.86 (2 H, d, J = 6.0 Hz), 4.19 (2 H, t, J = 7.3 Hz), 1.77 (2 H, m),1.23 (2 H, m), 0.88 (3 H, t, J = 7.6 Hz). ¹³C NMR (100 MHz, DMSO- d_6): δ 136.11, 131.83, 122.56, 120.56, 50.84, 48.61, 31.32, 18.79, 13.31. Anal. Calcd for C₁₀H₁₇N₂Br: C, 48.99; H, 6.99; N, 11.43. Found: C, 48.84; H, 7.18; N, 11.40. 1-Allyl-3butylimidazolium bromide (3.00 g, 12.2 mmol) was charged to a 250 mL round-bottomed flask, and DI water (30 mL) was added along with a magnetic stir bar. A solution of lithium bis(trifluoromethylsulfonyl)imide (3.69 g, 12.9 mmol) in DI water (40 mL) was added, and the resulting mixture was stirred at room temperature overnight. Chloroform (50 mL) was added, and the mixture was transferred to a separatory funnel where the organic layer was separated and washed with DI water (3 × 30 mL) and the solvent removed under reduced pressure, resulting in a light yellow oil (5.25 g, 96%). ¹H NMR (400 MHz, DMSO- d_6): δ 9.18 (1 H, s), 7.81 (1 H, s), 7.73 (1 H, s), 6.04 (2 H, m), 5.36 (2 H, m), 4.84 (2 H, d, J = 6.4 Hz), 1.78 (2 H, m), 1.25 (2 H, m), 0.90 (3 H, t, J = 7.3 Hz). ¹³C NMR (100 MHz, DMSO- d_6): δ 136.10, 131.77, 122.60, 120.15, 50.92, 48.67, 31.32, 18.81, 13.26. Anal. Calcd for $C_{12}H_{17}F_6N_3O_4S_2$: C, 32.36; H, 3.85; N, 9.43; S, 14.40. Found: C, 32.52; H, 3.83; N, 9.48; S, 14.42.

Preparation of 1-Hexenyl-3-methylimidazolium bis-(trifluoromethylsulfonyl)imide [NTf₂] 1q. N-Methylimidazole (2.00 g, 24.4 mmol) and 6-bromohex-1-ene⁴⁸ (4.36 g, 26.8 mmol) were dissolved in acetonitrile (30 mL). The resulting homogeneous mixture was stirred magnetically at 70 °C overnight. The volatiles were then removed under reduced pressure to afford a viscous yellow oil, which was subsequently washed with diethyl ether (3 × 30 mL) and dried in a vacuum oven (50 °C, < 0.01 mmHg) overnight, resulting in 1-hexenyl-3-methylimidazolium bromide as a viscous yellow oil (5.56 g, 93%). ¹H NMR (400 MHz, DMSO- d_6): δ 9.31 (1 H, s), 7.84 (1 H, s), 7.77 (1 H, s), 5.76 (2 H, m), 5.00 (2 H, m), 4.20 (2 H, d, J = 7.3 Hz), 3.87 (3 H, s), 2.03 (2 H, m), 1.78 (2 H, m), 1.31 (2 H, m). ¹³C NMR (100 MHz, DMSO- d_6): δ 138.10, 136.49, 123.55, 122.21, 115.18, 48.48, 35.75, 32.38, 28.90, 24.65. Anal. Calcd for C₁₀H₁₇N₂Br: C, 48.99; H, 6.99; N, 11.43. Found: C, 49.10; H, 7.02; N, 11.34. In a 250 mL roundbottomed flask was dissolved 1-hexenyl-3-methylimidazolium bromide (2.90 g, 11.8 mmol) in DI water (25 mL). To this magnetically stirred solution was added a solution of lithium bis(trifluoromethylsulfonyl)imide (3.57 g, 12.4 mmol) in DI water (30 mL). The resulting solution was stirred overnight at room temperature; then chloroform (50 mL) was added. The organic layer was separated, washed with DI water (3 \times 30 mL), and dried in vacuo to give 1-hexenyl-3-methylimidazolium [NTf₂] 1g as a light yellow oil (4.85 g, 92%). ¹H NMR (400 MHz, DMSO- d_6): δ 9.10 (1 H, s), 7.76 (1 H, s), 7.69 (1 H, s), 5.78 (2 H, m), 5.00 (2 H, m), 4.16 (2 H, d, J = 7.1 Hz), 3.84 (3 H, s), 2.05 (2 H, q, J = 6.8 Hz), 1.78 (2 H, m), 1.33 (2 Hz)H, m). ¹³C NMR (100 MHz, DMSO- d_6): δ 138.11, 136.52, 123.66, 122.27, 119.50 (q, J = 319 Hz, $-CF_3$), 48.63, 35.76, 32.45, 28.93, 24.72. Anal. Calcd for C₁₂H₁₇F₆N₃O₄S₂: C₁ 32.36; H, 3.85; N, 9.43; S, 14.40. Found: C, 32.52; H, 3.82; N, 9.49; S, 14.28.

Preparation of 1-Decenyl-3-methylimidazolium bis-(trifluoromethylsulfonyl)imide [NTf₂] **1h**. 1-Bromo-9-decene⁴⁹ (2.48 g, 10.1 mmol) and N-methylimidazole (0.75 g, 9.14 mmol) were dissolved in acetonitrile (20 mL) and stirred magnetically at 60 °C for 3 days. The solvent was then removed under reduced pressure, affording a crude yellow oil. The crude product was washed with petroleum ether (3×30) mL) and dried in a vacuum oven (50 °C, < 0.01 mmHg), resulting in 1-decenyl-3-methylimidazolium bromide, a viscous, light yellow oil (2.81 g, 93%). ¹H NMR (400 MHz, DMSO d_6): δ 9.21 (1 H, s), 7.80 (1 H, s), 7.73 (1 H, s), 5.77 (2 H, m), 4.95 (2 H, m), 4.14 (2 H, t, J = 7.1 Hz), 3.84 (3 H, s), 1.99 (2 H, m), 1.77 (2 H, m), 1.31 (10 H, m). 13C NMR (100 MHz, DMSO- d_6): δ 138.78, 136.49, 123.58, 122.25, 114.69, 48.70, 35.75, 33.16, 28.45, 28.40, 28.33, 28.20, 25.48. Anal. Calcd for C₁₄H₂₅BrN₂: C, 55.81; H, 8.36; N, 9.30. Found: C, 55.74; H, 8.45; N, 9.45. 1-Decenyl-3-methylimidazolium bromide (2.00 g, 6.07 mmol) was dissolved in DI water (20 mL) in a 100 mL round-bottomed flask. To this magnetically stirred solution was added a solution of lithium bis(trifluoromethylsulfonyl)imide (1.92 g, 6.68 mmol) in DI water (20 mL). The resulting solution was stirred overnight at room temperature; then chloroform (50 mL) was added. The organic layer was separated, washed with DI water (3 \times 30 mL), and dried in vacuo to give 1-decenyl-3-methylimidazolium [NTf₂] 1h as a light yellow oil (3.09 g, 96%). ¹H NMR (400 MHz, DMSO d_6): δ 9.09 (1 H, s), 7.76 (1 H, s), 7.70 (1 H, s), 5.78 (2 H, m), 4.97 (2 H, m), 4.14 (2 H, t, *J* = 7.1 Hz), 3.84 (3 H, s), 2.00 (2 H, m), 1.77 (2 H, m), 1.32 (10 H, m). 13C NMR (100 MHz, DMSO- d_6): δ 138.83, 136.51, 123.64, 122.29, 119.51 (q, J =320 Hz, -CF₃), 114.70, 48.78, 35.76, 33.21, 29.39, 28.66, 28.43, 28.36, 28.24, 25.49. Anal. Calcd for C₁₆H₂₅F₆N₃O₄S₂: C, 38.32; H, 5.02; N, 8.38; S, 12.79. Found: C, 38.38; H, 5.00; N, 8.36; S, 12.72.

Photopolymerization Procedure. UV curing of thiolene polymer networks was conducted following a previously published procedure from our laboratories.⁴⁶ The thiol/ene functional group ratio was stoichiometric for all photopolymerizations. The ene monomer functionality was held constant at a mole ratio of 1.5:1.0 bis/mono. As an example, PIL network PIL-C4 was prepared by dissolving 1 wt % of the photoinitiator DMPA (17.1 mg) in PTMP (0.53 g, 1.09 mmol). 1,3-Bisallylimidazolium [NTf₂] (0.70 g, 1.63 mmol) and 1-allyl-3-butylimidazolium [NTf₂] 1b (0.48 g, 1.09 mmol) were then added, and the mixture was shaken using a vortex mixer until a homogeneous solution was obtained (1-2 min). The solution was dispensed by syringe between two Rain-X treated glass slides, separated by a 500 µm PTFE spacer and held together by binder clips, and then exposed to a broadband UV lamp (UVP Blak-Ray B-100AP High-Intensity UV Lamp) for 5 min on each side. Polymer samples were then removed and stored in a vacuum oven (60 °C, < 0.01 mmHg) for 24 h prior to any polymer analysis. Duplicate specimens of each PIL were produced. For the system employing 1-allyl-3-icosylimidazolium $[NTf_2]$ 2f, the polymerization was completed at 60 °C, above the melting point of the monomer.

Fourier Transform Infrared Spectroscopy (FTIR). Spectra were recorded on a PerkinElmer Spectrum Two FT-IR in transmission mode. The PerkinElmer Spectrum 10 software was used to follow the desired peaks at 1 cm⁻¹ resolution using 32 scans. Thiol (2570 cm⁻¹) and double bond (1630 cm⁻¹) conversions were determined from multiple FTIR spectra taken for each thiol—ene network specimen

Scheme 1. Synthesis of Monofunctional "Ene" Monomers with Variable Terminal Alkyl Chain

Scheme 2. Synthesis of Monofunctional "Ene" Monomers Bearing a Variable Alkyl Tether

before and after UV curing. Functional group conversions were determined from peak areas, normalized to a peak unaffected by the polymerization reaction, using the following equation: degree of conversion = $(A_o - A_t)/A_o$, where A_o and A_t are the normalized peak areas before and after the polymerization, respectively.⁵⁰ Error in measurements was determined to be less than ±2%. An overlay of representative FT-IR spectra for each PIL can be found in the Supporting Information (Figure

Polymer Characterization. Cured PIL networks were subjected to Soxhlet extraction in refluxing THF (24 h) according to a previously published method.⁵¹ A TA Instruments Q200 differential scanning calorimeter (DSC), at a heating rate of 2 °C/min on 4-8 mg samples, was utilized to determine the T_g values of the PIL networks. Glass transition temperatures (T_{σ}) were determined from the second heating cycle by the inflection point of the observed curve. All DSC T_g experiments were performed in duplicate on each sample with an error of ±2.0 °C for a total of four measurements per PIL formulation. Thermal stability $(T_{d5\%})$ values were recorded in duplicate for each PIL sample using a TA Instruments Q500 thermogravimetric analyzer (TGA) under a constant nitrogen flow at a heating rate of 10 °C/min using TGA. $T_{d5\%}$ is defined as the temperature at which 5% weight loss of the polymer sample was observed. Representative DSC and TGA curves for each PIL network are provided in the Supporting Information (Figures S9-S11). A TA Instruments Q800 dynamic mechanical analyzer (DMA) in film tension mode with a single frequency of 1 Hz at a heating rate of 5 °C/min was used to determine the mechanical properties of the PIL network films. Values reported are from the second heating event for each PIL specimen (total of four measurements per formulation). Elemental analysis was completed in triplicate (using the instrumentation previously described) on each PIL specimen, the results of which are provided in Table S1.

X-ray Scattering Analysis. Temperature-dependent X-ray scattering experiments were performed in transmission mode on a Ganesha 300 XL SAXS system (SAXSLAB) with a Linkam HFS 350 variable temperature stage (Linkam Instruments) and a TMS94 liquid nitrogen pump for temperature stabilization under a constant flow of nitrogen. Prior to the measurement, each sample was cooled to -50 °C and then heated to 50 °C. The temperature of the sample was controlled by the Linkam stage from -50 to 50 °C with a step size of 10 °C (heating rate = 10 °C min⁻¹) and an equilibration time of 20 min before data collection (acquisition time = 5 min). The X-ray source of this laboratory-based system was a GeniX^{3D} Cu LF, a collimated X-ray beam delivery system (Xenocs), providing a microfocused beam at $\lambda = 1.54$ Å. The scattering data were recorded with an EIGER R 1 M detector (Dectris).

Dielectric Relaxation Spectroscopy (DRS). DRS measurements were performed with an in-house, custom-built, twoelectrode cell (Figure S16) and a Metrohm FRA32 M frequency response analyzer. The cell was placed inside a controlled-temperature/humidity chamber (Espec BTU-433), set to a relative humidity of 30%. Circular disks of ~12 mm in diameter were cut from the PIL films (500 μ m thickness), each of which was pretreated in a vacuum oven (<0.01 mmHg, 60 °C) for 24 h prior to assembly. The disks were sandwiched between two 304L stainless steel electrodes, separated by a 500 um PTFE spacer. The electrodes/sample were held both concentrically and under compression using two CNCmachined PTFE mounts and two stainless steel caps; six 4-40 bolts/nuts were tightened to 3 in-lb with a torque driver. Dielectric permittivity and conductivity were measured isothermally in steps of 10 °C over a frequency range of $0.1-10^7$ Hz with an ac amplitude of ± 0.01 V. Samples were soaked at each individual temperature until a constant conductivity was observed (45-50 min). The DC conductivity (σ_{DC}) was determined from the plateau value observed in the spectral dependence of the conductivity function ($\sigma' = \omega \varepsilon'' \varepsilon_0$ where ω is the frequency, ε'' is the dielectric loss, and ε_o is the vacuum permittivity). Representative plots of log σ' versus log ω for each PIL formulation can be found in the Supporting Information (Figures S17–S24).

RESULTS AND DISCUSSION

Monomer Synthesis and Thiol-Ene Photopolymerization. A series of monofunctionalized "ene" monomers, containing an imidazolium group with either a variable terminal or tether alkyl chain, were prepared initially. While the synthesis of 1-allyl-3-methylimidazolium [NTf₂] 1a has been previously reported,⁴⁷ the remaining ionic liquid

Scheme 3. Preparation of Covalently Crosslinked Poly(ionic liquid) Networks Using Thiol-Ene Photopolymerization

Table 1. Gel Fraction Data and Thermal Properties of the Thiol-Ene PIL Networks

polymer ID	gel fraction	% swelling	DSC T_g (°C)	TGA $T_{d5\%}$ (°C)
PIL-STD	$96.5 \pm 2.1\%$	$152 \pm 3\%$	-5.0 ± 0.8	353
PIL-C1	$92.2 \pm 0.2\%$	$156 \pm 1\%$	-19.4 ± 0.4	341
PIL-C4	$92.5 \pm 0.4\%$	$162 \pm 4\%$	-26.2 ± 0.8	351
PIL-C8	$93.5 \pm 1.3\%$	$177 \pm 5\%$	-30.6 ± 1.2	349
PIL-C12	$93.6 \pm 0.5\%$	$185 \pm 2\%$	-24.3 ± 0.9	350
PIL-C16	$90.4 \pm 0.2\%$	$199 \pm 7\%$	$-14.8 \pm 0.9 \ (T_{\rm m} = 1.3 \pm 0.2)$	359
PIL-C20	$83.4 \pm 0.5\%$	$218 \pm 6\%$	$-8.7 \pm 0.8 \ (T_{\rm m} = 32.1 \pm 0.3)$	347
PIL-HEX	$93.0 \pm 0.4\%$	$167 \pm 8\%$	-22.3 ± 0.5	355
PIL-DEC	$91.7 \pm 0.6\%$	$186 \pm 8\%$	-26.6 ± 0.6	341

monomers bearing a terminal alkyl chain were prepared as shown in Scheme 1. First, N-allylimidazole was quaternized with a 1-bromoalkane of the desired chain length (C4, C8, C12, C16, C20), generating a series of 1-allyl-3-alkylimidazolium bromides. Standard anion exchange conditions with lithium bis(trifluoromethylsulfonyl)imide (LiNTf₂) were then followed in order to generate the targeted monofunctional "ene" [NTf₂] ionic liquids 1b–1f. All of the monomers were room-temperature ionic liquids except for 1f, which was a solid with a melting point of 33 °C.

The remaining monomers where the variable alkyl chain was tethered between the main polymer chain and the imidazolium group were prepared as shown in Scheme 2. To prepare 1-hexenyl-3-methylimidazolium [NTf₂] 1g, 1,6-dibromohexane was first allowed to react with potassium *tert*-butoxide, generating 6-bromohex-1-ene after fractional distillation. His was then reacted with N-methylimidazole to produce 1-hexenyl-3-methylimidazolium bromide and further converted into 1-hexenyl-3-methylimidazolium [NTf₂] 1g after anion exchange with LiNTf₂. 1-Decenyl-3-methylimidazolium [NTf₂] 1h was synthesized by first converting 9-decen-1-ol to 10-bromodecene with PBr₃ followed by reaction with N-methylimidazole and anion exchange with LiNTf₂.

Covalently cross-linked thiol—ene PIL networks were prepared stoichiometrically according to thiol/ene functional groups with a 1.5:0.5 molar ratio of 1,3-bisallylimidazolium [NTf₂]⁴⁶ to monofunctional IL monomer 1a–1g (Scheme 3). DMPA (2,2-dimethoxy-2-phenylacetophenone) was used as the photoinitiator (1 wt %). Once prepared, the resulting homogeneous monomer mixture was dispensed by syringe between two glass slides, separated by a PTFE spacer of 500 μ m thickness, and photopolymerized for 5 min on each side using a broadband UV lamp. The resulting films were clear with varying degrees of yellow color and flexibility. Analysis by

FT-IR spectroscopy revealed a high degree of functional group conversion (<2% thiol (2570 cm⁻¹) remaining and no detectable alkene (1630 cm⁻¹) signal; Figure S8) across all of the PIL films prepared. The networks were found to be insoluble across a wide series of conventional organic solvents (acetone, THF, CH₂Cl₂, CHCl₃, CH₃OH, DMF, DMSO). Going forward, PIL networks are identified using the notation "PIL-X" where "X" refers to the type of monofunctional monomer used. For example, "C1" refers to the monomer 1a where a terminal methyl group was employed, whereas "HEX" refers to monomer 1g, which contains a hexyl alkyl tether (after polymerization).

Gel Fraction Analysis and Thermal Properties of Thiol-Ene PIL Networks. To further probe the degree of network formation in these "hybrid" PILs, gel fraction analysis was completed on each film using THF as the solvent. As shown in Table 1, all of the PIL networks exhibited a high gel fraction (>90%) except PIL-C20, which exhibited a more moderate gel fraction (~83%). For reference, data from a standard "backbone" poly(ionic liquid) network (PIL-STD), prepared using a stoichiometric thiol/ene functional group ratio of 1,3-bisallylimidazolium [NTf2] and PTMP (no monofunctional monomer), is included. To further probe the lower gel fraction exhibited by the PIL-C20 network, the THF extract from the gel fraction experiment was analyzed using ¹H NMR and FTIR spectroscopy. The results indicated that the extract contained C20-enriched oligomeric material with a negligible concentration (<2% by FTIR) of unreacted ene end groups. PIL network swelling was found to gradually increase with increasing pendant alkyl chain length (C1 to C20), which is attributed to an enhancement in polymer-solvent interactions as the network becomes more nonionic/hydrophobic.

Within the series PIL-C1 through PIL-C20, DSC T_{α} values showed a parabolic-like dependency upon the length of the terminal alkyl chain length (Figure 1). Starting with a value of

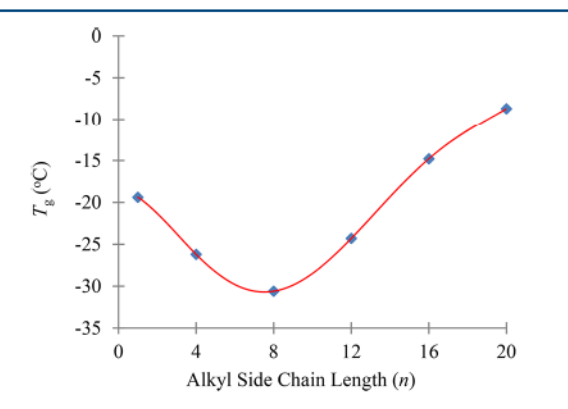


Figure 1. Effect of pendant alkyl chain length on T_g .

-19.8 °C for PIL-C1, $T_{\rm g}$ steadily decreased to -30.2 °C for PIL-C8 due to a decrease in cross-link density and the plasticizing ability of the growing terminal alkyl chain. When the terminal alkyl chain was lengthened further, $T_{\rm g}$ was found to increase steadily up to -8.7 °C for PIL-C20. An increase in van der Waals interactions between longer side chains appears to cause this remarkable increase in T_g . Further emphasizing the development of significant noncovalent, side chain interactions, the PIL-C16 and PIL-C20 networks were found to exhibit a melting transition in addition to a T_g (Table 1). Moving the alkyl chain spacer from a terminal position to a tether between the alkene and imidazolium group resulted in only a T_g being observed, both of which were significantly lower than PIL-STD, again due to a decrease in cross-link density. In general, thermogravimetric analysis of the PIL networks indicated thermal stability $(T_{d5\%})$ values well within the range of previously reported imidazolium [NTf2] PILs. All PILs were found to be thermally stable >340 °C with no discernible structural correlation with which a monofunctional monomer was used.

Mechanical Properties of Thiol-Ene PIL Networks. Mechanical properties of the PIL networks were analyzed by dynamic mechanical analysis (DMA; Figure 2). Rubbery plateau moduli (E' at 100 °C) were found to be in the range of 1.86-2.87 MPa across all of the films which employed a

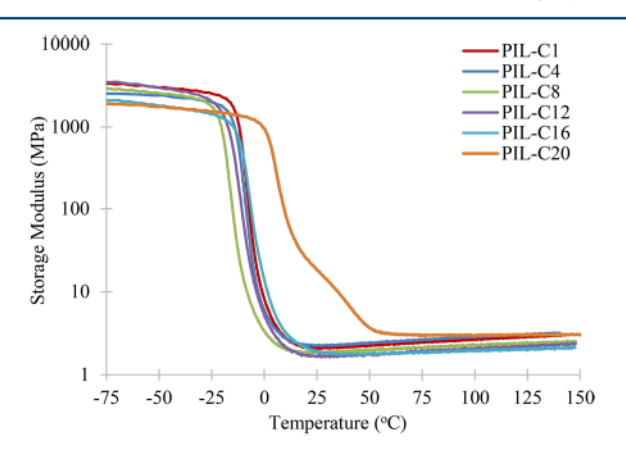


Figure 2. Overlay of storage modulus (E') as a function of temperature for PILs containing a variable terminal alkyl chain.

monofunctional monomer with no discernible correlation with the structure of the monofunctional monomer. This was expected as the overall thiol/ene functional group ratio was held stoichiometric across all formulations. DMA T_g values, determined from the maximum of the tan δ curves (Figure \$12), mirrored the relationships deduced from DSC analysis. For the PILs which utilized a monofunctional monomer with a terminal alkyl chain, DMA T_g was found to decrease from C1 to C8 and then increase to a final chain length of C20. Both the storage modulus and $\tan \delta$ curves for PIL-C20 indicate that the network may not be completely homogeneous and suggests microphase separation given the moderately high gel fraction observed (~83%). Additional insight into the nanostructure of the C20 system will be discussed in greater detail later with respect to X-ray scattering data as the storage modulus data appears to indicate the existence of microdomains within the network. All of the PILs were found to exhibit lower E' and DMA T_{σ} values than the standard PIL (STD), confirming the idea that the "hybrid PILs" are less cross-linked than the purely "backbone PIL." PILs where the alkyl chain acted as a tether between the main chain and the imidazolium group also exhibited mechanical properties that were generally lower in terms of both E' and DMA T_g when compared with the standard thiol-ene PIL (Figures S13 and S14). Apparent cross-link densities (ρ_x) of the PIL networks were determined following rubbery elasticity theory ($\rho_x = E'/3RT$), ⁴⁶ resulting in values in the range of $(2.0-3.1) \times 10^{-4}$ mol/cm³.

X-ray Scattering Results for the Thiol-Ene PIL Networks. Due to the unique thermal and mechanical properties observed for the PIL networks bearing longer terminal alkyl chains, the nanostructures of several PIL networks were studied by temperature-controlled X-ray scattering. Temperature-dependent X-ray scattering curves of the pertinent PIL networks (q = 0.05-2 Å) are presented in Figure 3 and additional information can be found in the Supporting Information (see Figure S15 and Table S2). Correlation lengths d_n are defined by $2\pi/q_n$. All of the PIL networks investigated here, regardless of which IL monomers were used, exhibited two wide-angle scattering peaks (labeled q_3 and q_4) at $q \sim 0.8$ and 1.4 Å⁻¹, implying that those peaks are associated with the 3D network structure. The scattering peak q_4 (d_4 of ~ 4.5 Å) has been observed in previous PIL studies and can be assigned generally to the amorphous halo. 19,29,52-54 This mean correlation distance represents a combination of several features of the system, including the π - π interactions between neighboring imidazolium rings, van der Waals interactions between alkyl chains, and other intramolecular relationships.¹⁹ With an increase in temperature, a very small increase in d_4 was observed, implying a small thermal dilatation of the polymeric structures upon heating. This increase is slightly more abrupt in PIL-C16 and PIL-C20 as the sample temperature crosses the melting transition.

The scattering peak q_3 represents the anion-to-anion correlation distance (d_3) , which, like d_4 , is a common correlation distance for PILs. $^{52-56}$ As with d_4 , little variability was observed in d_3 with temperature except as the $T_{\rm m}$ was approached for PIL-C16 and PIL-C20. A slight decrease in d_4 occurred (given a constant T) as the terminal alkyl chain length was increased. A similar, more pronounced decrease in d_3 was observed. This trend, which is unique to the covalently cross-linked PIL networks studied here, seems to indicate that the ionic groups are being forced closer together as the nonpolar region in the network cavity gets larger. Previous PIL

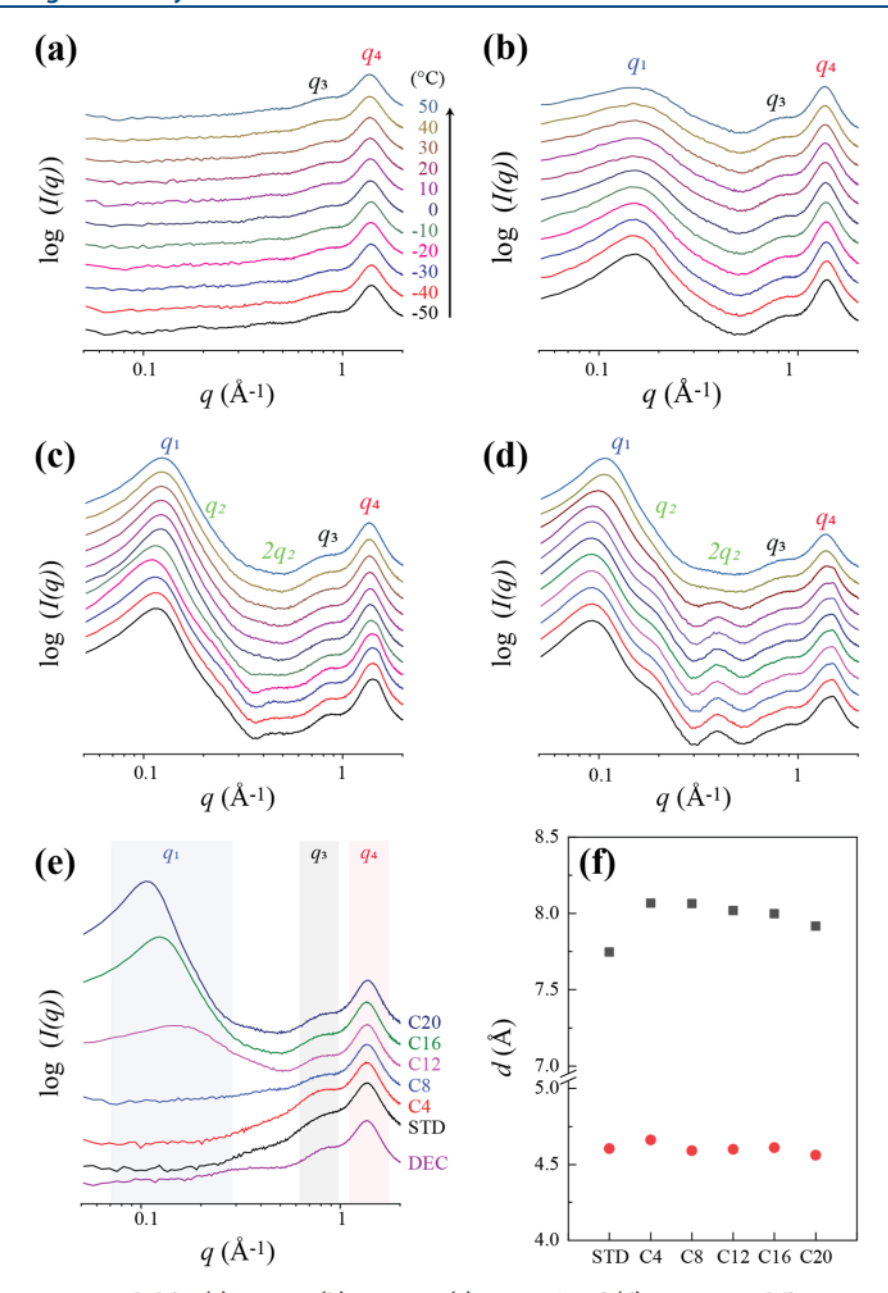


Figure 3. X-ray scattering curves recorded for (a) PIL-C8, (b) PIL-C12, (c) PIL-C16, and (d) PIL-C20 at different temperatures. Part e shows an overlay of scattering data taken for each PIL at 50 °C, while part f is a plot of distance (d₃ in black; d₄ in red) as a function of terminal alkyl chain length at 50 °C. A table of correlation distances as a function of temperature for selected PILs is provided as Table S2.

work with poly(1-alkyl-3-vinylimidazolium [NTf₂]) homopolymers and other related (meth)acrylate PIL copolymers and homopolymers showed that increasing the terminal alkyl chain length resulted in little to no observable shift in the amorphous halo scattering peak (d_4) and a general increase in the anionto-anion correlation distance (d_3) as noncovalently crosslinked chains have the mobility to accommodate larger nonpolar domains, resulting in a larger and weaker separation between anions.²⁹

Several of the PIL networks exhibited additional scattering peaks: (i) PIL-C12 had one additional small-angle scattering peak (q_1) ; (ii) PIL-C16 and PIL-C20 showed three additional small-angle scattering peaks (q_1, q_2) and its secondary peak (q_2) . The q_2 scattering peak is assigned to the backbone-to-backbone correlation distance $(d_2)^{52-56}$ and was only observed in PIL-C16 and PIL-C20. The d_2 distance increased as the

length of alkyl chains on the respective monofunctional monomers increased (29.0 to 32.5 Å), of which the length scale in this work is comparable to the actual length of alkyl chains. Moreover, d_2 disappeared above the $T_{\rm m}$ implying that the crystal structures defining the distance between backbones dissembled. On the basis of these observations, it was concluded that only long alkyl chains on the monofunctional monomers (C16, C20) that have the ability to interdigitate between backbones, forming chain-extended crystallites, in the PIL network voids. The alkyl chains become no longer interdigitated above $T_{\rm m}$, resulting in a loss of the backbone-to-backbone correlation distance as exhibited by the disappearance of q_2 . Since the other PIL networks have shorter alkyl chains and cannot form an interdigitated crystallite domain, this behavior was only observed in PIL-C16 and PIL-C20.

To the best of our knowledge, q_1 has not been observed for non-network PILs. One distinguishable feature of q_1 from q_2 is that the peak does not vanish even when the temperature is higher than $T_{\rm m}$. Additionally, the length scale of d_1 is much larger than d_2 but is still dependent upon the length of alkyl chains. Thus, d_1 is presumably related to the correlation distance among nanodomains formed by the aggregation of pendant alkyl chains surrounded by charges as suggested by Triolo et al. in his work on imidazolium IL structures. 5

Conductive Properties of Thiol-Ene PIL Networks. The ionic conductivity of the PIL networks was evaluated using dielectric relaxation spectroscopy (DRS). The complex dielectric permittivity $\sigma^*(\omega,T)$ was measured under isothermal conditions over a temperature range from 30 to 150 °C at 30% RH in 10 °C steps in the 0.1-10⁷ Hz frequency range. The plateau value observed in the spectral dependence of the real conductivity ($\sigma' = \omega \varepsilon'' \varepsilon_0$ where ω is the frequency, ε'' is the dielectric loss, and ε_0 is the vacuum permittivity) was used to determine the DC-conductivity (σ_{DC} ; Figures S17-S24). Figure 4 (top) shows the σ_{DC} values for the PILs containing

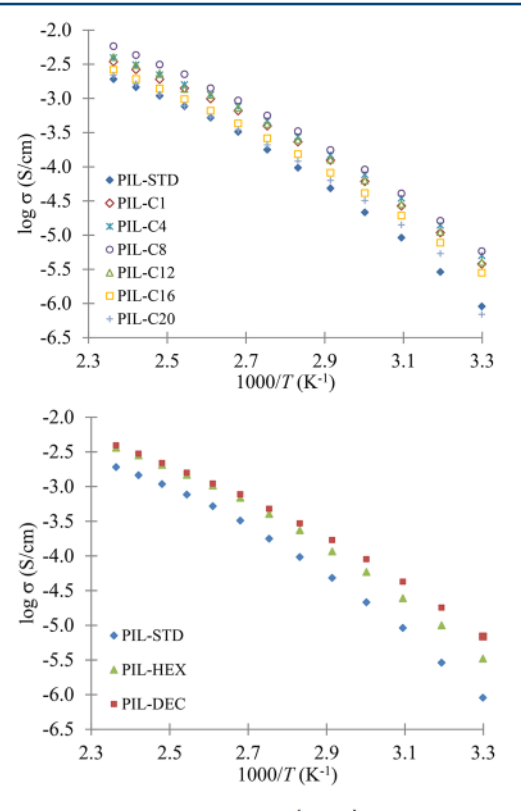


Figure 4. Overlay of log conductivity (S/cm) versus 1000/T at 30% RH for PILs (top) containing a variable terminal alkyl chain and (bottom) containing a variable alkyl tether.

a variable terminal alkyl chain, as a function of reciprocal temperature. It is immediately worth noting that all of the PILs in this grouping exhibited a higher ionic conductivity than the purely "backbone PIL" (PIL-STD), which is attributed to a less cross-linked network as well as a slightly higher mol % IL content in the "hybrid" PIL networks (Tables 2 and 3). PIL-C20 exhibited an unexpectedly low ionic conductivity at 30 °C; however this reading was taken below the $T_{\rm m}$ (32.1 °C). Additional readings taken above the T_m for PIL-C20 indicated that this material behaved similarly to its analogous PILs.

Table 2. Mechanical Properties of the Thiol-Ene PIL Networks As Determined from Dynamic Mechanical **Analysis**

polymer ID	E' @ 100 °C (MPa)	$\tan \delta \max (^{\circ}C)$	$\rho_x \times 10^{-4} (\text{mol/cm}^3)$
PIL-STD	9.12 ± 0.45	3.5 ± 0.6	9.80 ± 0.04
PIL-C1	2.87 ± 0.21	-3.9 ± 0.5	3.08 ± 0.02
PIL-C4	2.37 ± 0.47	-6.3 ± 0.7	2.55 ± 0.05
PIL-C8	2.55 ± 0.22	-10.7 ± 1.3	2.74 ± 0.02
PIL-C12	1.86 ± 0.17	-7.8 ± 0.4	2.00 ± 0.02
PIL-C16	1.95 ± 0.05	-5.0 ± 0.4	2.10 ± 0.01
PIL-C20	2.53 ± 0.38	7.4 ± 0.6	2.72 ± 0.04
PIL-HEX	2.31 ± 0.35	-8.8 ± 0.4	2.48 ± 0.04
PIL-DEC	2.15 ± 0.15	-12.6 ± 0.3	2.31 ± 0.02

Table 3. Ionic Conductivity at 30 °C, 30% RH, and VFT Fitting Parameters of Poly(ionic liquid) Networks

polymer ID	mol % IL	σ (S/cm) 30 °C, 30% RH	$\frac{\sigma_{\rm o}~({ m S}/{ m cm})}{ m cm}$	B (K)	T ₀ (K)
PIL-STD	54.2	9.1×10^{-7}	1.6	1470	201
PIL-C1	61.7	3.8×10^{-6}	1.7	1404	196
PIL-C4	60.8	5.0×10^{-6}	1.9	1406	194
PIL-C8	59.8	6.5×10^{-6}	6.3	1654	183
PIL-C12	58.8	4.0×10^{-6}	3.6	1603	187
PIL-C16	58.0	2.8×10^{-6}	3.3	1748	178
PIL-C20	57.3	6.9×10^{-7}	2.2	1638	186
PIL-HEX	60.7	3.3×10^{-6}	2.2	1440	196
PIL-DEC	59.4	6.9×10^{-6}	1.7	1436	188

Overall, ionic conductivities of the PIL networks with variable terminal alkyl chains correlated inversely with T_{σ} as follows: C8 > C4 > C12 > C1 > C16 > C20. As the alkyl chain length increases from C1 to C8, an increase in ionic conductivity is observed and is attributed to the plasticizing effect that the small to moderate alkyl chains have on the relatively rigid cross-linked network. With greater flexibility, polymer chain relaxation is more easily attainable, leading to improved ion transport. However, upon further increasing the alkyl chain from C8 to C20, we see a steady decrease in ionic conductivity. As demonstrated previously from the X-ray scattering data, longer alkyl chains begin to form nonionic lamella within the voids of the polymer network. The observed decrease in ionic conductivity upon moving from PIL-C8 to PIL-C20 is a direct result of the anions being forced to navigate around these nonionic regions. For the PILs containing the variable alkyl tether (Figure 4), a modest increase in ionic conductivity was also observed compared with the "backbone PIL" network. In fact, PIL-DEC exhibited the highest ionic conductivity of all the PILs reported here (6.9 × 10⁻⁶ S/cm at 30 °C, 30% RH). Although longer tether chains were not investigated, it is assumed that by placing the spacer as a tether rather than in a terminal position, the formation of larger, nonionic voids from alkyl chain organization can be avoided, leading to improved conductivity.

The ionic conductivities of these systems followed Vogel-Fulcher-Tammann (VFT) dependence for all of the PILs (except for the 30 °C reading for PIL-C20, which was below the melting temperature) according to the following equation:

$$\sigma_{\rm DC} = \sigma_{\rm o} \exp(-B/(T - T_{\rm o}))$$

where σ_0 is the high temperature ionic conductivity limit, B is the fitting parameter related to the activation energy of ionic conduction, and T_0 is the Vogel temperature. Such fitting is attributed to the relationship that exists between long-range diffusion of ionic species and their coupling to polymer chain relaxation dynamics. VFT fitting parameters can be found in

As differences in ionic conductivities appear to be decreasing with increasing temperature, suggesting that changes in T_g becomes less influential, normalization of the curves with T_{σ} was completed (Figure 5). Such universal scaling of

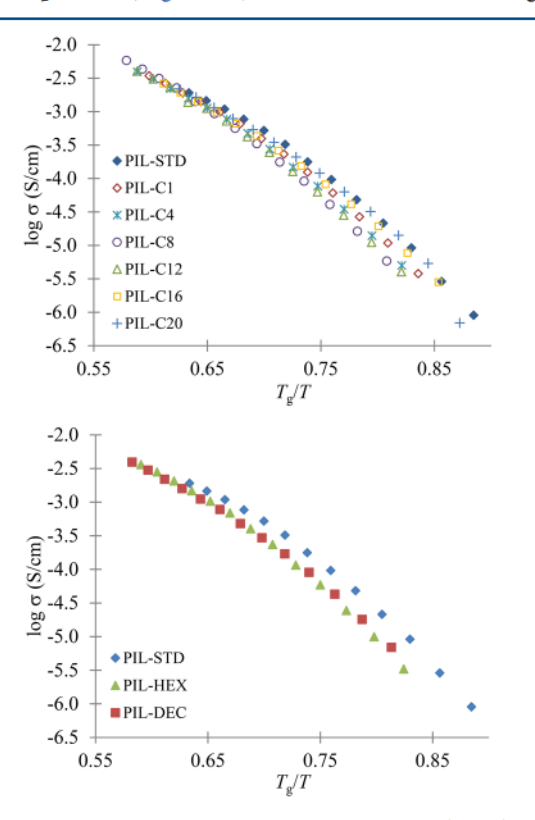


Figure 5. T_{σ} -normalized overlay of log conductivity (S/cm) versus $T_{\rm e}/T$ at 30% RH for PILs (top) containing a variable terminal alkyl chain and (bottom) containing a variable alkyl tether.

conductivity for PILs and neat ILs has been accomplished through the normalization of $T_{\rm g}$ in order to account for differences in polymer segmental motion. $^{40,58-60}$ After normalization, the curves do not completely collapse onto one another, indicating that T_g may not be the only factor affecting ionic conductivity and ion transport. In fact, the conductivities appear to have inverted, with the PIL-STD system exhibiting the highest T_g-independent ionic conductivity and PIL-C8 exhibiting the lowest T_g -independent ionic conductivity. Although additional experimentation is necessary, this observation is supported by the recent hypothesis that purely "backbone" PILs exhibit ionic conductivities that are less T_{σ} dependent due to more regular spacing of the ions, thus generating a more correlated path of charge transport. 40 The data collected as part of this study suggest that some level of aggregation may be present in the "hybrid" PILs; however, since the overall range of ionic conductivities observed for these networks is relatively small, it is difficult to further decipher any subtle relationships with respect to ion spacing, ion pair aggregation/dissociation, and other related factors.

CONCLUSIONS

Poly(ionic liquid) networks containing backbone and pendant imidazolium groups ("hybrid PILs") were prepared using thiol-ene "click" photochemistry. Pendant imidazolium groups were incorporated into the PIL networks through the synthesis of monofunctional "ene" monomers that contained either a terminal alkyl group at N-3 of variable length (R = C1, C4, C8, C12, C16, or C20) or a variable alkyl tether spacer (n= 6 or 10) between the newly formed C-S bond and the imidazolium ring. Thermal analysis of the resulting PIL networks found an interesting correlation between the length of the terminal alkyl spacer and T_g . As the terminal alkyl chain length increased from C1 to C8, a decrease in T_{σ} was observed, presumably due to a plasticizing effect of the pendant chain. However, upon further increasing the chain length up to C20, a gradual increase in T_{σ} occurred. The formation of chainextended crystallites within the non-ionic regimes in the network cavities is thought to be the result of this increase in $T_{\rm g}$ and the observance of $T_{\rm m}$ values for PIL-C16 and PIL-C20. This hypothesis was further supported by X-ray scattering data through the observance of the q_2 scattering peak, which was assigned to a backbone-to-backbone distance that results from the interdigitation of the C16 and C20 alkyl chain lengths. Such a peak was not observed for any PIL where the alkyl chain length was below C16, including the PILs with variable alkyl tether spacer and the purely "backbone" PIL-STD. Furthermore, the q_2 scattering peak disappears above $T_{\rm m}$, implying that this distance becomes disassembled upon melting. Ionic conductivities of the networks were determined from dielectric relaxation spectroscopy, and a correlation with T_{σ} was observed at lower temperatures. As the temperature was increased, the curves began to coalesce, indicating less of a dependence on T_g and the networks dynamics. The purely "backbone" PIL-STD system exhibited the highest T_{g} independent ionic conductivity, although the "hybrid" systems were not dramatically affected. This might indicate a high degree of ion percolation within the "hybrid" PIL networks. Further experimentation is necessary to elucidate the more complex ion transport mechanism(s) that exist(s) in these systems.

ASSOCIATED CONTENT

Supporting Information

The Supporting Information is available free of charge on the ACS Publications website at DOI: 10.1021/acs.iecr.8b04720.

Additional synthetic methods and ¹H and ¹³C NMR spectra for all IL monomers; FTIR and elemental analysis data, DSC thermograms, and TGA traces for all PILs as well as DMA storage modulus and tan δ curves for PIL-HEX and PIL-DEC; X-ray scattering curves recorded for PIL-STD and PIL-C4 at different temperatures along with a table of correlation distances of the PIL networks at various temperatures; additional DRS data including representative $\log \sigma'$ vs $\log \omega'$ plots as a functional of temperature for each PIL network (PDF)

AUTHOR INFORMATION

Corresponding Author

*E-mail: kmiller38@murraystate.edu.

ORCID

Sung-Soo Kim: 0000-0001-7871-3869

Christopher J. Ellison: 0000-0002-0393-2941 Kevin M. Miller: 0000-0001-5314-7477

Notes

The authors declare no competing financial interest.

ACKNOWLEDGMENTS

This contribution was identified by Dr. Timothy Long (Virginia Tech) as the Best Presentation in the "Ionic Liquids in Polymer Science & Engineering: From Molecular Design to Energy & Beyond" session of the 2018 ACS Fall National Meeting in Boston. This work was supported by a Research in Undergraduate Institutions (RUI) award from the National Science Foundation, Division of Materials Research, Polymers Program (DMR-1708632). Thermal and mechanical analyses were conducted in the Polymer and Materials Science Laboratory (PMCL) at Murray State University. DMA support was provided by the Department of Chemistry at Murray State University as a result of support from the National Science Foundation (Major Research Instrumentation) under DMR-1427778. Parts of this work were carried out in the Characterization Facility, University of Minnesota, which receives partial support from NSF through the MRSEC program.

■ REFERENCES

- (1) Mecerreyes, D. Polymeric Ionic Liquids: Broadening the Properties and Applications of Polyelectrolytes. *Prog. Polym. Sci.* 2011, 36, 1629–1648.
- (2) Yuan, J.; Mecerreyes, D.; Antonietti, M. Poly(ionic liquid)s: An Update. *Prog. Polym. Sci.* 2013, 38, 1009–1036.
- (3) Shaplov, A. S.; Marcilla, R.; Mecerreyes, D. Recent Advances in Innovative Polymer Electrolytes based on Poly(ionic liquid)s. *Electrochim. Acta* 2015, 175, 18–34.
- (4) Qian, W.; Texter, J.; Yan, F. Frontiers in Poly(ionic liquid)s: Syntheses and Applications. Chem. Soc. Rev. 2017, 46, 1124-1159.
- (5) Bara, J. E.; Lessmann, S.; Gabriel, C. J.; Hatakeyama, E. S.; Noble, R. D.; Gin, D. L. Synthesis and Performance of Polymerizable Room-Temperature Ionic Liquids as Gas Separation Membranes. *Ind. Eng. Chem. Res.* 2007, 46, 5397–5404.
- (6) Tomé, L. C.; Gouveia, A. S. L.; Freire, C. S. R.; Mecerreyes, D.; Marrucho, I. M. Polymeric Ionic Liquid-Based Membranes: Influence of Polycation Variation on Gas Transport and CO₂ Selectivity Properties. *J. Membr. Sci.* 2015, 486, 40–48.
- (7) Carlisle, T. K.; Wiesenauer, E. F.; Nicodemus, G. D.; Gin, D. L.; Noble, R. D. Ideal CO₂/Light Gas Separation Performance of Poly(vinylimidazolium) Membranes and Poly(vinylimidazolium)-Ionic Liquid Composite Films. *Ind. Eng. Chem. Res.* 2013, 52, 1023–1032.
- (8) Cowan, M. G.; Gin, D. L.; Noble, R. D. Poly(ionic liquid)/Ionic Liquid Ion-Gels with High "Free" Ionic Liquid Content: Platform Membrane Materials for CO₂/Light Gas Separations. *Acc. Chem. Res.* 2016, 49, 724–732.
- (9) Ran, J.; Wu, L.; Varcoe, J. R.; Ong, A. L.; Poynton, S. D.; Xu, T. Development of Imidazolium-type Alkaline Anion Exchange Membranes for Fuel Cell Application. *J. Membr. Sci.* 2012, 415–416, 242–249.
- (10) Liu, L.; He, S.; Zhang, S.; Zhang, M.; Guiver, M. D.; Li, N. 1,2,3-Triazolium-Based Poly(2,6-Dimethyl Phenylene Oxide) Copolymers as Anion Exchange Membranes. ACS Appl. Mater. Interfaces 2016, 8, 4651–4660.
- (11) Margaretta, E.; Fahs, G. B.; Inglefield, D. L., Jr.; Jangu, C.; Wang, D.; Heflin, J. R.; Moore, R. B.; Long, T. E. Imidazolium-Containing ABA Triblock Copolymers as Electroactive Devices. ACS Appl. Mater. Interfaces 2016, 8, 1280–1288.
- (12) Wu, H.; Kuang, M.; Cui, L.; Tian, D.; Wang, M.; Luan, G.; Wang, J.; Jiang, L. Single-Material Solvent-Sensitive Actuator from

- Poly(ionic liquid) Inverse Opals Based on Gradient Dewetting. Chem. Commun. 2016, 52, 5924–5927.
- (13) Appetecchi, G. B.; Kim, G.-T.; Montanino, M.; Carewska, M.; Marcilla, R.; Mecerreyes, D.; De Meatza, I. Ternary Polymer Electrolytes Containing Pyrrolidinium-Based Polymeric Ionic Liquids for Lithium Batteries. *J. Power Sources* **2010**, *195*, 3668–3675.
- (14) Shaplov, A. S.; Ponkratov, D.; Vlasov, P.; Lozinskaya, E.; Gumileva, I.; Surcin, C.; Morcrette, M.; Armand, M.; Aubert, P.-H.; Vidal, F.; Vygodskii, Y. Ionic Semi-interpenetrating Networks as a New Approach for Highly Conductive and Stretchable Polymer Materials. J. Mater. Chem. A 2015, 3, 2188–2198.
- (15) Grygiel, K.; Lee, J.-S.; Sakaushi, K.; Antonietti, M.; Yuan, J. Thiazolium Poly(ionic liquid)s: Synthesis and Application as Binder for Lithium-Ion Batteries. *ACS Macro Lett.* 2015, 4, 1312–1316.
- (16) Zhang, P.; Li, M.; Yang, B.; Fang, Y.; Jiang, X.; Veith, G. M.; Sun, X. G.; Dai, S. Polymerized Ionic Networks with High Charge Density: Quasi-Solid Electrolytes in Lithium-Metal Batteries. *Adv. Mater.* 2015, 27, 8088–8094.
- (17) Ayalneh Tiruye, G.; Munoz-Torrero, D.; Palma, J.; Anderson, M.; Marcilla, R. All-solid State Supercapacitors Operating at 3.5V by using Ionic Liquid Based Polymer Electrolytes. *J. Power Sources* 2015, 279, 472–480.
- (18) Ohno, H. Molten Salt Type Polymer Electrolytes. *Electrochim. Acta* 2001, 46, 1407–1411.
- (19) Chen, H.; Choi, J.-H.; Salas-de la Cruz, D.; Winey, K. I.; Elabd, Y. A. Polymerized Ionic Liquids: The Effect of Random Copolymer Composition on Ion Conduction. *Macromolecules* 2009, 42, 4809–4816.
- (20) Lee, M.; Choi, U. H.; Colby, R. H.; Gibson, H. W. Ion Conduction in Imidazolium Acrylate Ionic Liquids and their Polymers. *Chem. Mater.* 2010, 22, 5814–5822.
- (21) Green, M. D.; Salas-de la Cruz, D.; Ye, Y.; Layman, J. M.; Elabd, Y. A.; Winey, K. I.; Long, T. E. Alkyl-Subsituted N-Vinylimidazolium Polymerized Ionic Liquids: Thermal Properties and Ionic Conductivities. *Macromol. Chem. Phys.* 2011, 212, 2522–2528.
- (22) Weber, R. L.; Ye, Y.; Banik, S. M.; Elabd, Y. A.; Hickner, M. A.; Mahanthappa, M. K. Thermal and Ion Transport Properties of Hydrophilic and Hydrophobic Polymerized Styrenic Imidazolium Ionic Liquids. J. Polym. Sci., Part B: Polym. Phys. 2011, 49, 1287—1296
- (23) Ye, Y.; Elabd, Y. A. Anion Exchanged Polymerized Ionic Liquids: High Free Volume Single Ion Conductors. *Polymer* 2011, *52*, 1309–1317.
- (24) Choi, U. H.; Lee, M.; Wang, S. R.; Liu, W. J.; Winey, K. I.; Gibson, H. W.; Colby, R. H. Ionic Conduction and Dielectric Response of Poly(imidazolium acrylate) Ionomers. *Macromolecules* 2012, 45, 3974–3985.
- (25) Ye, Y.; Choi, J.; Winey, K. I.; Elabd, Y. A. Polymerized Ionic Liquid Block and Random Copolymers: Effect of Weak Microphase Separation on Ion Transport. *Macromolecules* 2012, 45, 7027–7035.
- (26) Choi, J.; Ye, Y.; Elabd, Y. A.; Winey, K. I. Network Structure and Strong Microphase Separation for High Ion Conductivity in Polymerized Ionic Liquid Block Copolymers. *Macromolecules* 2013, 46, 5290-5300.
- (27) Fan, F.; Wang, Y.; Hong, T.; Heres, M. F.; Saito, T.; Sokolov, A. P. Ion Conduction in Polymerized Ionic Liquids with Different Pendant Groups. *Macromolecules* 2015, 48, 4461–4470.
- (28) Iacob, C.; Matsumoto, A.; Brennan, M.; Liu, H.; Paddison, S. J.; Urakawa, O.; Inoue, T.; Sangoro, J.; Runt, J. Polymerized Ionic Liquids: Correlation of Ionic Conductivity with Nanoscale Morphology and Counterion Volume. *ACS Macro Lett.* 2017, 6, 941–946.
- (29) Delhorbe, V.; Bresser, D.; Mendil-Jakani, H.; Rannou, P.; Bernard, L.; Gutel, T.; Lyonnard, S.; Picard, L. Unveiling the Ion Conduction Mechanism in Imidazolium-Based Poly(ionic liquids): A Comprehensive Investigation of the Structure-to-Transport Interplay. *Macromolecules* 2017, 50, 4309–4321.
- (30) Matsumoto, A.; Iacob, C.; Noda, T.; Urakawa, O.; Runt, J.; Inoue, T. Introducing Large Counteranions Enhances the Elastic

- Modulus of Imidazolium-Based Polymerized Ionic Liquids. *Macromolecules* 2018, 51, 4129-4142.
- (31) Mogurampelly, S.; Keith, J. R.; Ganesan, V. Mechanisms Underlying Ion Transport in Polymerized Ionic Liquids. *J. Am. Chem. Soc.* 2017, 139, 9511–9514.
- (32) Sangoro, J. R.; Iacob, C.; Agapov, A. L.; Wang, Y.; Berdzinski, S.; Rexhausen, H.; Strehmel, V.; Friedrich, C.; Sokolov, A. P.; Kremer, F. Decoupling of Ionic Conductivity from Streutural Dynamics in Polymerized Ionic Liquids. *Soft Matter* 2014, *10*, 3536–3540.
- (33) Wojnarowska, Z.; Feng, H.; Fu, Y.; Cheng, S.; Carroll, B.; Kumar, R.; Novikov, V. N.; Kisliuk, A. M.; Saito, T.; Kang, N.-G.; Mays, J. W.; Sokolov, A. P.; Bocharova, V. Effect of Chain Rigidity on the Decoupling of Ion Motion from Segmental Relaxation in Polymerized Ionic Liquids: Ambient and Elevated Pressure Studies. *Macromolecules* 2017, 50, 6710–6721.
- (34) Wojnarowska, Z.; Knapik, J.; Diaz, M.; Ortiz, A.; Ortiz, I.; Paluch, M. Conductivity Mechanism in Polymerized Imidazolium-Based Protic Ionic Liquid [HSO₃–BVIm][OTf]: Dielectric Relaxation Studies. *Macromolecules* 2014, 47, 4056–4065.
- (35) Williams, S. R.; Salas-de la Cruz, D.; Winey, K. I.; Long, T. E. Ionene Segmented Block Copolymers Containing Imidazolium Cations: Structure-Property Relationships as a Function of Hard Segment Content. *Polymer* 2010, *51*, 1252–1257.
- (36) Lee, M.; Choi, U. H.; Salas-de la Cruz, D.; Mittal, A.; Winey, K. I.; Colby, R. H.; Gibson, H. W. Imidazolium Polyesters: Structure-Property Relationships in Thermal Behavior, Ionic Conductivity, and Morphology. *Adv. Funct. Mater.* 2011, 21, 708–717.
- (37) Williams, S. R.; Wang, W.; Winey, K. I.; Long, T. E. Synthesis and Morphology of Segmented Poly(tetramethylene oxide)-Based Polyurethanes Containing Phosphonium Salts. *Macromolecules* 2008, 41, 9072–9079.
- (38) Gao, R.; Zhang, M.; Wang, S.; Moore, R. B.; Colby, R. H.; Long, T. E. Polyurethanes Containing an Imidazolium Diol-Based Ionic-Liquid Chain Extender for Incorporation of Ionic-Liquid Electrolytes. *Macromol. Chem. Phys.* 2013, 214, 1027–1036.
- (39) Choi, U. H.; Mittal, A.; Price, T. L., Jr.; Colby, R. H.; Gibson, H. W. Imidazolium-Based Ionic Liquids as Initiators in Ring Opening Polymerization: Ionic Conduction and Dielectric Response of End-Functional Polycaprolactones and their Block Copolymers. *Macromol. Chem. Phys.* 2016, 217, 1270–1281.
- (40) Evans, C. M.; Bridges, C. R.; Sanoja, G. E.; Bartels, J.; Segalman, R. A. Role of Tethered Ion Placement on Polymerized Ionic Liquid Structure and Conductivity: Pendant versus Backbone Charge Placement. ACS Macro Lett. 2016, 5, 925–930.
- (41) Hall, L. M.; Seitz, M. E.; Winey, K. I.; Opper, K. L.; Wagener, K. B.; Stevens, M. J.; Frischknecht, A. L. Ionic Aggregate Structure in Ionomer Melts: Effect of Molecular Architecture on Aggregates and the Ionomer Peak. J. Am. Chem. Soc. 2012, 134, 574–587.
- (42) Hall, L. M.; Stevens, M. J.; Frischknecht, A. L. Dynamics of Model Ionomer Melts of Various Architectures. *Macromolecules* 2012, 45, 8097–8108.
- (43) Ting, C. L.; Stevens, M. J.; Frischknecht, A. L. Structure and Dynamics of Coarse-Grained Ionomer Melts in an External Electric Field. *Macromolecules* 2015, 48, 809–818.
- (44) Kim, S.; Miller, K. M. Synthesis and Thermal Analysis of Crosslinked Imidazolium-Containing Polyester Networks Prepared by Michael Addition Polymerization. *Polymer* 2012, 53, 5666–5674.
- (45) Whittington, C. P.; Daily, L. A.; Miller, K. M. Crosslinked Imidazolium-Containing Polyester Networks Containing a Pendant Imidazolium Group: Swelling Studies and Thermal Properties. *Polymer* 2014, 55, 3320–3329.
- (46) Rhoades, T. C.; Wistrom, J. C.; Johnson, R. D.; Miller, K. M. Thermal, Mechanical and Conductive Properties of Imidazolium-Containing Thiol-ene Poly(ionic liquid) Networks. *Polymer* 2016, 100, 1–9.
- (47) Wang, G.; Fang, S.; Liu, Y.; Luo, D.; Yang, L.; Hirano, S. Physicochemical Properties of Functionalized 1,3-Dialkylimidazolium Ionic Liquids Based on the Bis(fluorosulfonyl)imide Anion. *RSC Adv.* 2016, 6, 66650–66657.

- (48) Lübbe, C.; Dumrath, A.; Neumann, H.; Beller, M.; Kadyrov, R. Lewis Acid Assisted Ruthenium-Catalyzed Metathesis Reactions. *ChemCatChem* 2014, 6, 105–108.
- (49) Motesharei, K.; Myles, D. C. Molecular Recognition on Functionalized Self-Assembled Monolayers of Alkanethiols on Gold. *J. Am. Chem. Soc.* 1998, 120, 7328–7336.
- (50) Shanmuganathan, K.; Elliot, S. M.; Lane, A. P.; Ellison, C. J. highly Stretchable Thermoset Fibers and Nonwovens Using Thiol-ene Photopolymerization. ACS Appl. Mater. Interfaces 2014, 6, 14259—14265.
- (51) Mather, B. D.; Miller, K. M.; Long, T. E. Novel Michael Addition Networks Containing Poly(propylene glycol) Telechelic Oligomers. *Macromol. Chem. Phys.* 2006, 207, 1324–1333.
- (52) Salas-de la Cruz, D.; Green, M. D.; Ye, Y.; Elabd, Y. A.; Long, T. E.; Winey, K. I. Correlating Backbone-to-Backbone Distance to Ionic Conductivity in Amorphous Polymerized Ionic Liquids. J. Polym. Sci., Part B: Polym. Phys. 2012, 50, 338–346.
- (53) Allen, M. H.; Wang, S.; Hemp, S. T.; Chen, Y.; Madsen, L. A.; Winey, K. I.; Long, T. E. Unveiling the Ion Conduction Mechanism in Imidazolium-Based Poly(ionic liquids): A Comprehensive Investigation of the Structure-to-Transport Interplay. *Macromolecules* 2013, 46, 3037–3045.
- (54) Nakamura, K.; Fukao, K.; Inoue, T. Dielectric Relaxation and Viscoelastic Behavior of Polymerized Ionic Liquids with Various Counteranions. *Macromolecules* 2012, 45, 3850–3858.
- (55) Liu, H.; Paddison, S. J. Direct Comparison of Atomistic Molecular Dynamics Simulations and X-Ray Scattering of Polymerized Ionic Liquids. *ACS Macro Lett.* 2016, 5, 537–543.
- (56) Liu, H.; Paddison, S. J. Alkyl Chain Length Dependence of Backbone-to-Backbone Distance in Polymerized Ionic Liquids: An Atomistic Simulation Perspective on Scattering. *Macromolecules* 2017, 50, 2889–2895.
- (57) Triolo, A.; Russina, O.; Bleif, H.-J.; Di Cola, E. Nanoscale Segregation in Room Temperature Ionic Liquids. *J. Phys. Chem. B* 2007, 111 (18), 4641–4644.
- (58) Hoarfrost, M. L.; Segalman, R. A. Ionic Conductivity of Nanostructured Block Copolymer/Ionic Liquid Membranes. *Macromolecules* 2011, 44, 5281–5288.
- (59) Hoarfrost, M. L.; Segalman, R. A. Conductivity Scaling Relationships for Nanostructured Block Copolymer/Ionic Liquid Membranes. ACS Macro Lett. 2012, 1, 937–943.
- (60) Sangoro, J. R.; Iacob, C.; Serghei, A.; Friedrich, C.; Kremer, F. Universal Scaling of Charge Transport in Glass-forming Ionic Liquids. *Phys. Chem. Chem. Phys.* 2009, *11*, 913–916.